This article has been accepted for publication in a future issue of this journal, but has not been fully edited. Content may change prior to final publication. Citation information: DOI 10.1109/JBHI.2020.3012567, IEEE Journal of Biomedical and Health Informatics

A Novel Automated Blood Pressure Estimation Algorithm Using Sequences of Korotkoff Sounds

Ahmadreza Argha, *Member, IEEE,* Branko G. Celler, *Fellow, IEEE,* and Nigel H. Lovell, *Fellow, IEEE*

***Abstract*—The use of automated non-invasive blood pressure (NIBP) measurement devices is growing, as they can be used without expertise and BP measurement can be performed by patients at home. Non-invasive cuff-based monitoring is the dominant method for BP measurement. While the oscillometric technique is most common, a few automated NIBP measurement methods have been developed based on the auscultatory technique. Amongst artificial intelligence (AI) techniques, deep learning has received increasing attention in different fields due to its strength in data classification and feature extraction problems. This paper proposes a novel automated AI-based technique for NIBP estimation from auscultatory waveforms (AWs) based on converting the NIBP estimation problem to a sequence-to-sequence classification problem. To do this, a sequence of segments was first formed by segmenting the AWs and their corresponding decomposed detail and approximation parts obtained by wavelet packet decomposition method, and extracting features from each segment. Then, a label was assigned to each segment, i.e. (*i*) between systolic and diastolic segments and (*ii*) otherwise, and a bidirectional long short term memory recurrent neural network (BiLSTM-RNN) was devised to solve the resulting sequence-to-sequence classification problem. Adopting a 5-fold cross-validation scheme and using a data base of 350 NIBP recordings gave an average mean absolute error of 1.7 ± 3.7 mmHg for systolic BP (SBP) and 3.4 ± 5.0 mmHg for diastolic BP (DBP) relative to reference values. Based on the results achieved and comparisons made with the existing literature, it is concluded that the proposed automated BP estimation algorithm based on deep learning methods and auscultatory waveform brings plausible benefits to the field of BP estimation.**

***Index Terms*—Deep learning based blood pressure estimation, bidirectional LSTM-RNN, systolic and diastolic blood pressure estimation, oscillometric waveform, auscultatory waveform, automated non-invasive blood pressure measurement.**

I. Introduction

CONTINUOUS beat-to-beat invasive blood pressure (IBP) is in fact the most important physiological signal obtained in critical care and cardiac surgery, where high accuracy and sensitivity are crucial. To measure BP invasively, an intra-arterial catheter is placed into the brachial artery. This requires a skilled clinician and can carry risk of complications including infection, bleeding and ischemia [1]. Alternatively, non-invasive BP (NIBP) measurement using Korotkoff sounds is widely used for BP estimation. In the so-called auscultatory technique, which was introduced in 1905 and is based on listening for the Korotkoff sounds, a stethoscope is used by a skilled observer to estimate the systolic and diastolic BP (SBP and DBP) values. This method has become widely accepted as a gold standard for NIBP [2], [3] calibration and is based on traditional sphygmomanometry [4] using an inflatable cuff, a stethoscope, and a manometer. The cuff is inflated to a pressure value well above the presumed SBP, referred to as suprasystolic pressure so that the artery under the cuff is completely occluded. The cuff is then gradually deflated and the pressures at which sounds produced by the arterial pulse waves (Korotkoff sounds) appear and disappear are noted by expert observers. The cuff pressure at which the first Korotkoff sound is heard defines the SBP and the pressure at which the sounds disappear or become muffled defines the DBP.

Measurement of BP is now widely carried out by automated NIPB monitoring devices. While NIBP monitors can be built based on both auscultatory and oscillometric techniques, the majority of the available monitors on the market today are based on the oscillometric technique [5]–[8], because of its simplicity and robustness. Similar to the auscultatory technique, the oscillometric method requires the inflation of an occluding cuff beyond the anticipated systolic pressure. As the cuff deflates, the oscillometric waveforms (OWs) which are pressure oscillations superimposed on the cuff pressure deflation wave are sensed by a pressure sensor. The OWs are recorded and processed to produce the so-called oscillometric waveform envelope (OWE).

It has however been shown that oscillometric NIBP measurements are less accurate than the auscultatory ones [9], [10], and the automated SBP and DBP estimates using OW are not very reliable, as OWE may be disturbed by cardiac arrhythmia which is very likely for elderly patients [11], [12]. Due to these issues a few automated (or semi-automated) auscultatory NIBP monitoring devices have been developed.

In this paper, a novel deep learning based method for NIBP estimation is presented using the auscultatory waveform which can accurately estimate the NIBP in the presence of different kinds of noise such as motion artifact as well as background noise. We have previously published conference papers [13], [14] outlining machine learning methods we have recently developed for the automated estimation of BP from digitized and recorded auscultatory signals. This work will demonstrate that greater accuracy is possible when using an advanced feature extraction method as well as recurrent networks that have access to both past and future information of the feature sequences extracted from AWs.

II. Related Work, Motivations and Contributions

Majority of AI-based oscillometric NIBP estimation algorithms have mimicked the classical maximum amplitude algorithm (MAA), and attempted to extract features from OWE by which systolic and diastolic ratios are estimated using different AI-based algorithms such as Gaussian mixture model

A. Argha (corresponding author) and N. H. Lovell are with the Graduate School of Biomedical Engineering, B. G. Celler is with the School of Electrical Engineering and Telecommunications, UNSW, Sydney, NSW 2052, Australia, e-mail: {a.argha, n.lovell and b.celler}@unsw.edu.au.

This article has been accepted for publication in a future issue of this journal, but has not been fully edited. Content may change prior to final publication. Citation information: DOI 10.1109/JBHI.2020.3012567, IEEE Journal of Biomedical and Health Informatics

(GMM) and Gaussian mixture regression (GMR) [15], multiple linear regression (MLR) [16], support vector regression [16], feedforward neural networks (FFNNs) [17], and deep learning regression methods, i.e. deep belief networks (DBNs)-deep neural networks (DNNs) [18]. However, some investigators have recently started analyzing oscillometric pulses and extracting features from them to estimate SBP and DBP as the beats at which significant changes occur in the extracted features. Among these approaches, while some assume that the pulses are independent and the features are extracted from each beat and no beat-by-beat features are derived [19], others extract beat-by-beat features, i.e. features that describe the relationship between neighboring beats are derived and fed into a classification model. Additionally, a number of methods using oscillometric pulses use classification models such as DBN-DNN and FFNN that are unable to take into account the dependencies between beats, whilst others employ the classification methods which are capable of taking into account dependencies between beats, i.e. Hidden Markov Model (HMM) [7] and long-short-term-memory recurrent neural network (LSTM-RNN) [8].

It has been shown that oscillometric NIBP measurements are less accurate than the auscultatory ones [9], [10], and the automated SBP and DBP estimates using OW are not very reliable, as OWE may be disturbed by cardiac arrhythmias which are common for elderly patients [11], [12]. Due to these issues a few automated (or semi-automated) auscultatory NIBP monitoring devices have been developed. Several automated and semi-automated smart-phone auscultatory BP kits have been developed to measure NIBP or calibrate (assess the accuracy of) other marketed oscillometric NIBP monitors [20]–[23], named *Accutension*. In these kits, Korotkoff sounds from the tube of a stethoscope are fed into the smart-phone via a microphone plugged into the jack and a software (smart-phone app) is employed to process, visualize and record the Korotkoff sounds. The recorded sounds are then used to determine SBP and DBP, automatically or manually by trained users.

Identical to the methods proposed for NIBP estimation by oscillometric pulses, the methods developed for AI-based NIBP estimation from AW can be categorized into two classes: (1) methods that assume Korotkoff sounds are independent and classification models used are incapable of taking into account the dependencies between consecutive Korotkoff sounds [24]; (2) methods that extract features from AWs and employ classification methods that can take into account dependencies between beats, i.e. HMM [7], [14] and LSTM-RNN [13]. The method developed in this study to estimate NIBP from Korotkoff sound sequences belongs to the latter category.

Our novelties and contributions to the current literature can be summarized as follows. (1) Unlike the existing literature which focuses on the oscillometric waveform to estimate NIBP, this work used Korotkoff sound sequences to develop an AI-based NIBP estimation algorithm. (2) Different from our previous work [13], [14] which use an algorithmic technique for extracting time-domain beat-by-beat features from Korotkoff sounds while denoising them, this work used a signal segmentation technique to segment the Korotkoff sounds and their corresponding decomposed signals achieved by wavelet packet decomposition approach, and then extracted time-frequency domain features from each window. Using these extracted features, a sequence-to-sequence classification problem was formed, in which each window (segment) or more accurately feature vector extracted from each window is classified into two classes of (i) between systolic and diastolic and (ii) otherwise. This approach is very different from the current literature which uses the oscillometric waveform envelope to extract features and solve a regression problem to estimate systolic and diastolic ratios. (3) Unlike our previous work [13], [14] which use GMM-HMM and shallow undirectional RNNs, this study used deep bi-directional long short term memory (BiLSTM) recurrent networks, i.e. deep learning networks, obtained by stacking the recurrent layers, that can have access to both past and future information of the sequences of recorded Korotkoff sounds, to solve the achieved sequence-to-sequence classification problem, shown to give better performance and higher accuracy without requiring a pre-processing step to denoise the data. Compared to [13], [14], the proposed signal segmentation, feature extraction and bi-directional RNNs methods make the developed NIBP estimation algorithm independent of a sophisticated preprocessing step.

III. Methods

A. Protocols for evaluation/validation of deep learning based models

The international standards introduced to evaluate/validate automated NIBP monitors mainly use the mean error (ME), the mean absolute error (MAE) and the standard deviation of error (SDE) of the measurements obtained from the automated NIBP monitor relative to the corresponding references [25]. An automated NIBP monitor can meet the American National Standards Institute, the Association for the Advancement of Medical Instrumentation along with the International Organization for Standardization (ANSI/AAMI/ISO) standard if the obtained absolute value of ME and SDE over the dataset are equal or less than 5 mmHg and 8 mmHg, respectively. In contrast, the British Hypertension Society (BHS) protocol [26] categorizes an NIBP monitoring device as Grade A if the absolute values of the error of 60%, 85% and 95% of its measurements are less than or equal to 5 mmHg, 10 mmHg, and 15 mmHg, respectively. In addition, a device is categorized as Grade B (Grade C), if 50% (40%), 75% (65%) and 90% (85%) of the measurements fall within the absolute differences of 5, 10 and 15 mmHg, respectively, from the reference standard. If an NIBP monitor achieves results worse than the Grade C, it is categorized as Grade D.

B. Data-set

In this study, a data base of 350 NIBP recordings collected from a variety of subjects was used (UNSW Research Ethics Committee (HREC) approval Number: 12/11), using a single FDA approved NIBP device. Each NIBP record contains the cuff pressure deflation curve, the oscillometric waveforms and the Korotkoff sounds digitized at 500 samples per second.

The 350 data records were from 155 individual subjects,

This article has been accepted for publication in a future issue of this journal, but has not been fully edited. Content may change prior to final publication. Citation information: DOI 10.1109/JBHI.2020.3012567, IEEE Journal of Biomedical and Health Informatics

(87 male, 68 female) aged 52.0 ± 21.6 years (range 23-97). The mean age and variance of both male and female subjects were closely matched at 51.1 ± 20.3 and 53.1 ± 23.4 years, respectively. Arm circumference ranged from 19-35 cms. Systolic, diastolic and mean arterial pressures ranged $81-191$, $37-104$ and $56-118$ mmHg, respectively. This data-set was explained in more details in [27], [28].

C. Gold reference

The most detailed analysis of the spectral and temporal components of Korotkoff sounds [29], used wideband (0.1–2000 Hz) external pulse recording during cuff deflation, identifying three distinct phases of the Korotkoff sounds (K_1, K_2 and K_3). K_1 is a low-amplitude, low frequency signal < 20 Hz, that is present with cuff pressures above SBP; K_2 is a triphasic signal appearing at SBP and disappearing at diastolic pressure, which approximately corresponds to the audible Korotkoff sound and has frequency spectra in the range of $20-80$ Hz; K_3 appears with cuff pressure between SBP and DBP and continues to be present below DBP. The study found a marked resemblance between K_3 and intra-arterial pressure, and that the onset and disappearance of K_2 was closely correlated to SBP and DBP derived from auscultation, with mean values of SBP generally higher than SBP and lower than DBP derived from auscultation. Another finding was that the visual technique detects the onset (disappearance) of K_2 a few beats before (after) the Korotkoff sound becomes audible (inaudible) at SBP (DBP) and as a result gives closer values to intra-arterial BP determinations than the conventional auscultatory technique.

Furthermore, numerous studies [27], [28], [30] have demonstrated that there are also significant inter-operator differences in estimating BP using sphygmomanometry, especially with the determination of DBP [27], [28], [31]. Our previous studies [27], [28] suggest that the accuracy of auscultatory sphygmomanometry is dependent on (i) the sensitivity of the stethoscope, (ii) the hearing acuity of the operator, and (iii) the amplitude and particular waveform morphometry of the Korotkoff sounds. It was also shown in [27], [28] that complete silence occurs on average in less than 50% of cases, making the determination of DBP particularly unreliable when Korotkoff sounds are listened to with stethoscopes. It is worth noting that other studies in the literature of automatic or semi-automatic auscultatory NIBP estimation methods [20]–[23], showed also that visual auscultatory technique is significantly correlated with the manual auscultation. Due to the above mentioned reasons, in this study, the visual technique was used to provide systolic and diastolic BP references.

D. Preprocessing and feature extraction

Similar to the process of gold reference determination explained before, the collected Korotkoff sounds were high-pass filtered with a cut-off frequency of 20 Hz. The filtered Korotkoff sounds are referred to as auscultatory waveform (AW) hereinafter. The root mean square (RMS) energy of the Korotkoff signal was calculated using a moving average zero phase digital filter with a Hamming window of 100 ms width.

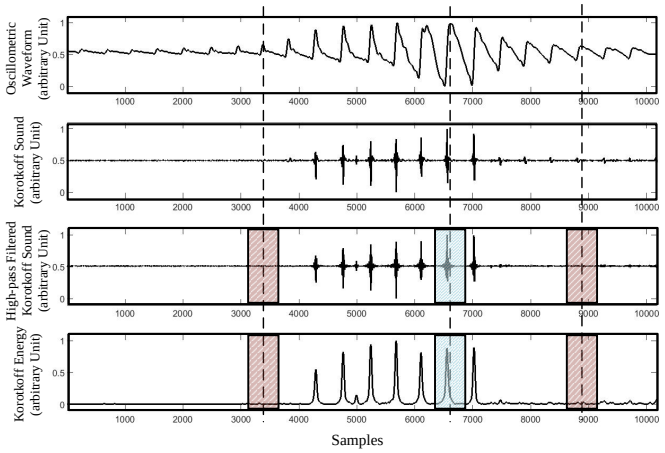

Fig. 1. Illustration of Korotkoff sound and energy segmentation. Detected peaks of oscillometric waveform were used as the center points for segmentation. Korotkoff sounds and energy were segmented into beat-by-beat frames (500 samples per frame).

RMS energy was previously used in [27] to improve the signal to noise ratio and provide a measure of background noise. The corresponding OW was further bandpass filtered to provide a bandwidth of 1.6-32 Hz and amplified it with a gain of 11,161 to improve the resolution. The bandpass filtering removes the linearly deflating baseline cuff pressure from the OW. The peaks of OW were detected and used as reference points to segment the AW into beat-by-beat AW frames. A window width of 1 s or equivalently 500 samples (sampling frequency was 500 Hz) was chosen, centered with each detected oscillometric peak. The same segmentation was applied to the energy waveform. An example of the AW segmentation is illustrated in Fig. 1. Wavelet packet decomposition (WPD) which is a multi-resolution analysis was used to decompose the high-pass filtered Korotkoff sound into low-frequency components (i.e. approximate part) and high-frequency components (i.e. detail parts). Identical to the aforementioned segmentation technique, each of the signals derived from the 5 level WPD with *Symlet 8* was segmented. The mean $\bar{x}_w$, standard deviation (SD, σ), mean of energy (i.e. $\frac{1}{n_w}\sum_{i=1}^{n_w} x_i^2$), maximum amplitude, skewness (i.e. $\frac{1}{n_w}\sum_{i=1}^{n_w}\left(\frac{x_i-\bar{x}_w}{\sigma}\right)^3$), Kurtosis (i.e. $\frac{1}{n_w}\sum_{i=1}^{n_w}\left(\frac{x_i-\bar{x}_w}{\sigma}\right)^4$), clearance factor (i.e. $\frac{Maximum-Amplitude}{\left(\frac{1}{n_w}\sum_{i=1}^{n_w}\sqrt{|x_i|}\right)^2}$), sample entropy (SampEn) and approximate entropy (ApEn) (with an embedding dimension of $m = 2$ and tolerance of $r = 0.2\sigma$) of each frame of Korotkoff energy were then calculated. The SD, kurtosis, skewness and clearance factor of each frame of the filtered Korotkoff sounds and their corresponding detail and approximate parts achieved by WPD were calculated. In addition to the aforementioned features, the ratio of the mean energy, the maximum amplitude of two consecutive frames were also calculated, i.e. $\frac{\text{mean of energy of } i-th \text{ frame}}{\text{mean of energy of } (i-1)-th \text{ frame}}$, $\frac{\text{mean of energy of } i-th \text{ frame}}{\text{mean of energy of } (i+1)-th \text{ frame}}$, $\frac{\text{maximum amplitude of } i-th \text{ frame}}{\text{maximum amplitude of } (i-1)-th \text{ frame}}$ and $\frac{\text{maximum amplitude of } i-th \text{ frame}}{\text{maximum amplitude of } (i+1)-th \text{ frame}}$. This last step generated 4 beat-by-beat time domain features. Finally, the cuff pressure corresponding to each oscillometric pulse was used as a feature as well. In total, 42 different features were extracted and

This article has been accepted for publication in a future issue of this journal, but has not been fully edited. Content may change prior to final publication. Citation information: DOI 10.1109/JBHI.2020.3012567, IEEE Journal of Biomedical and Health Informatics

used to train the deep learning model devised to perform the BP estimation using AW. To train the model faster, avoid saturation of the network, and further reduce the probability of becoming locked in local minima, the extracted features were normalized to $[0,\ 1]$.

E. NIBP estimation via classification of AW beats using deep learning

1) Forming a sequence-to-sequence classification problem: Each feature vector corresponding to AW beats was located in one of two classes, namely (*i*) between systolic and diastolic (BSD) and (*ii*) otherwise (OTW). The output target (class) corresponding to the i-th beat of the j-th record is denoted as $y_i \in \{1,\ 2\}$. Note that OTW $= 1$ and BSD $= 2$. The target sequence for the j-th record is formed as $Y_j = [y_1, y_2, \cdots, y_{n_j}]$. The SBP and DBP estimation problem from AWs was converted to a sequence-to-sequence classification problem as follows. First, a deep learning based classification model was developed to learn the nonlinear and complex relationship between the extracted feature vectors and the target labels and later classify each feature vector into two different classes, i.e. class 1 (OTW) and class 2 (BSD).

To identify the complex nonlinear relationship between the features (extracted from AWs) as described above, and the two phase target sequence, a bi-directional LSTM-RNN (BiLSTM-RNN) was devised. RNNs [32] are one of the NN architectures that have made significant breakthroughs in the machine learning field. RNNs are able to take sequential inputs and produce sequential outputs by sharing parameters between time steps. The LSTM-RNN [33] is a special kind of RNN obtained by replacing the activation function of the neurons to a unit with an ingenious inner structure called LSTM. LSTM can overcome the *vanishing gradient* problem of RNN by remembering information for long periods of time. The LSTM unit works as follows:

$$\begin{aligned} &f_t = \sigma(W_f x_t + U_f h_{t-1} + b_f),\ i_t = \sigma(W_i x_t + U_i h_{t-1} + b_i),\\ &o_t = \sigma(W_o x_t + U_o h_{t-1} + b_o),\ g_t = \tanh(W_g x_t + U_g h_{t-1} + b_g),\\ &c_t = f_t \circ c_{t-1} + i_t \circ g_t,\ h_t^f = o_t \circ \tanh(c_t), \end{aligned} \tag{1}$$

where $i,\ o,\ f,\ g$ and c are the input gate, output gate, forget gate, input of the cell, and the cell state, respectively, σ denotes the element-wise sigmoid function, $\{\circ\}$ denotes the Hadamard product, and h_t^f and c_t denote the forward hidden state vector (output of the LSTM unit) and explicit memory cell. Here, $U_f,\ U_i,\ U_o$ and $U_g \in \mathbb{R}^{N_h \times N_h}$ are the recurrent weights, where N_h denotes the number of LSTM units, $W_f,\ W_i,\ W_o$ and $W_g \in \mathbb{R}^{N_h \times M}$ are the input weights, where M denotes the number of inputs, i.e. $x_t \in \mathbb{R}^M$, and $b_f,\ b_i,\ b_o$ and $b_g \in \mathbb{R}^{N_h}$ are the bias weights. In undirectional LSTMs, the (forward) hidden state vector h_t^f captures information from the past history up to the present input, i.e. $[x_1, \cdots, x_{t-1}, x_t]$. However, it is possible to gain access to more temporal context of input sequences by incorporating future information, i.e. $[x_{t+1}, \cdots, x_{n_j}]$, which can inform the model of the downstream sequence. Bidirectional RNNs (BiRNNs) [34] were introduced to implement this idea by processing the data sequence in both forward and backward directions using two separate recurrent hidden layers, which then merge to the same output layer, i.e.

$$\begin{aligned} h_t^f &= \mathscr{H}\left(x_t, h_{t-1}^f, W^f\right),\\ h_t^b &= \mathscr{H}\left(x_t, h_{t-1}^b, W^b\right), \end{aligned} \tag{2}$$

where $\mathscr{H}(\cdot,\cdot,\cdot)$ denotes the equations in (1), h_t^f and h_t^b are the forward and backward hidden states, and W^f and W^b are the weights associated with the forward and backward hidden layers. The final vector of hidden states h is obtained by concatenating the outputs of the forward and backward LSTM layers as $h_t = \text{concat}\left(h_t^f, h_t^b\right)$. Several (Bi)LSTM layers can also be stacked to form a deeper recurrent network, shown to be able to outperform a shallow recurrent network [35]. The $(\ell+1)$-th $(\ell = 1, \cdots, L-1)$ recurrent layer can be formulated as

$$h_t^{\ell+1} = \mathscr{H}\left(x_t^{\ell+1}, h_{t-1}^{\ell+1}, W^{\ell+1}\right), \tag{3}$$

where

$$x_t^{\ell+1} = h_t^\ell + \beta^\ell x_t^\ell, \tag{4}$$

with $\beta^\ell \in \{0,1\}$ being a parameter that determines that a residual connection exits between the stacked layers, i.e. $\beta^\ell = 1$ if a residual connection exists and $\beta^\ell = 0$ otherwise. The output probabilities $\hat{y}$ are then calculated as

$$\hat{y}_t = \sigma\left(b_t + W_z\left(h_t^L + \beta^L x_t^L\right)\right). \tag{5}$$

For training the model, the following cross-entropy was minimized

$$J = -\sum_{i=1}^{N_m}\sum_{t=1}^{T_k} y_t \left(\log\ \hat{y}_t(W,b)\right) + \lambda \left\|\theta\right\|, \tag{6}$$

where N_m denotes the mini-batch size, and y_t and $\hat{y}_t(W,b)$ denote the target output and its predicted value, respectively, for the input x_t, on the given training data set using the back-propagation algorithm, and $\|\theta\|$ represents the L_2 norm of model parameters, i.e. θ, and λ denotes the corresponding penalty coefficient. Here, T_k denotes the length of the zero-padded sequences in the k-th $(k = 1, \cdots, \frac{N_{tr}}{N_m}$, with N_{tr} being the number of samples in the training data) mini-batch.

Although the number of features is the same for each sequence, input sequences are not of the same length, i.e. the number of Korotkoff sounds and as a result feature vectors vary in each NIBP sample. However, the developed deep learning model requires a fixed tensor as inputs, so during training, the training data was split into mini-batches and the sequences were post zero padded so that they have the same length. To minimize the negative impact of too much padding on the model performance, the $N_{tr} = 280$ training samples were first sorted based on their length, and then a mini-batch size of $N_m = 10$ was chosen (hence, we had 28 mini-batches), so that sequences in a mini-batch have a relatively similar length. Note that a 5-fold cross validation method was used, hence in each fold, 280 samples were used as the training data set and the remaining 70 samples used as the test data set. Masking, i.e. a matrix which contains zeros where the corresponding time steps are padding values and ones otherwise, was used to ensure that the padding values do not affect the loss calculations.

This article has been accepted for publication in a future issue of this journal, but has not been fully edited. Content may change prior to final publication. Citation information: DOI 10.1109/JBHI.2020.3012567, IEEE Journal of Biomedical and Health Informatics

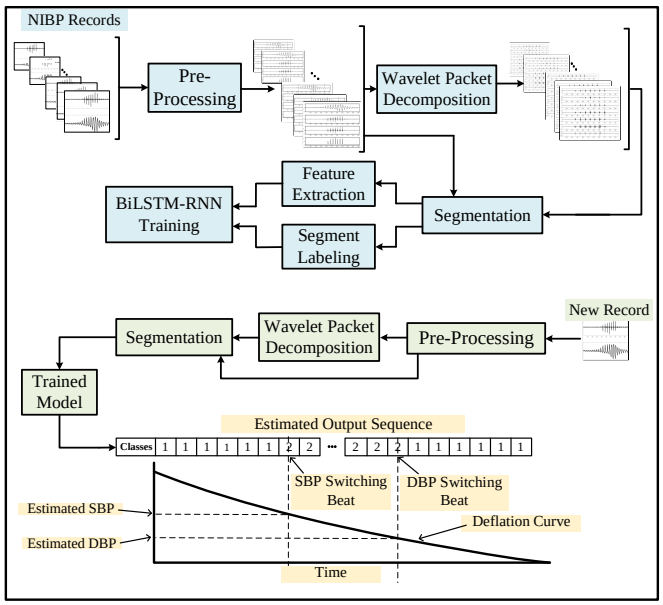

Fig. 2. Block diagram of the proposed deep learning based algorithm for SBP and DBP estimation.

2) SBP and DBP estimation from the estimated label sequences: The segment at which a detected target sequence switches from class 1 to 2 (from OTW to BSD) and later from class 2 to 1 (from BSD to OTW) were identified and the SBP and DBP were estimated by projecting the switching beats to the deflation curve to find their corresponding cuff pressure. The diagram of the proposed data-driven method to carry out the BP estimation from AWs is shown in Fig. 2.

IV. Results

A database of 350 NIBP records including auscultatory waveform, oscillometric waveform and cuff pressure deflation curve was used in this study. A 5-fold cross-validation (CV) scheme was used to evaluate the performance of the classification model proposed for BP estimation method, and hence the results reported in this paper have been obtained by averaging the five values yielded from 5 different trained models and test sample sets. Using extensive experiments, the hyper-parameters of the devised LSTM-RNNs were tuned on 80% of NIBP samples and validated on the remaining 20% samples, which can be seen in Table I.

Table II lists the results obtained by different LSTM-RNN classification models. Models 1 includes a BiLSTM layer with 75 units, Model 2 is an RNN model with two BiLSTM layers each of which with 75 LSTM units, Model 3 includes 2 BiLSTM layers (75 units) incorporated with residual connections, Model 4 has three stacked BilSTM layers (75 LSTM units in each layer), Model 5 has 3 stacked BiLSTM (each of which with 75 units) with skip connections, Model 6 has an undirectional LSTM layer with 75 units, and finally Model 7 is a model with three undirectional LSTM layers each of which included 75 units.

To check that the results achieved by the 5-fold cross-validation scheme will generalize to independent data sets, two other cross validation schemes were used as well; leave-one-out CV (LOOCV) and leave-one-subject-out CV (LOSOCV). The latter CV scheme was used to check that the achieved results are subject independent and was carried out by keeping all the samples from a single subject for validation and using the rest for training. As seen from Table I, the achieved results by these two CV schemes are very close to the ones achieved by the 5-fold CV scheme.

TABLE I
Parameter setting of the devised BiLSTM-RNN classification models.

Optimization algorithm	Adam
Initial learning rate	0.001
Gradient decay factor	0.9000
Squared gradient decay factor	0.9990
Mini-batch size	10
Number of epoch	100
L_2 regularization factor	0.001

A DBN-DNN classification model [36] was also trained with three hidden layers each of which included 75 neurons using these hyper-parameters: learning rate 0.05, momentum rate 0.9, mini-batch size 100, number of epoch in the pre-training 20, number of epoch in the fine-training 500, and L_2 regularization factor 0.0005. More details of the devised DBN-DNN can be seen in [19]. An FFNN classification model, with the same structure of the devised DBN-DNN classification model, was also trained by utilizing the resilient backpropagation (RB) training algorithm and setting the hyper-parameters to the ones used in [37]. The achieved results are given in Table II. The results achieved by the undirectional LSTM network and beat-by-beat time-domain features proposed in [13] are also given in Table II.

V. Discussion

As can be seen from Table II, the best results were obtained by Model 5, i.e. a BiLSTM-RNN model with three BiLSTM layers incorporated with residual connections. The results achieved in this study showed that (1) deep RNN architectures can outperform shallow RNNs [35], and (2) using the residual connection between adjacent recurrent layers in deep RNNs can further improve the results, as it effectively can avoid the exploding and vanishing gradient problems [38]. It is also evident from this table that most of the LSTM-RNN classification models investigated were able to achieve a BHS Grade A and an acceptable AAMI result in DBP estimation, whilst only those using BiLSTM layers could achieve a BHS Grade A and pass the AAMI protocol in terms of SBP estimation. In other words, the models with undirectional LSTM layers could not estimate SBP very accurately. This is basically due to the presence of noise in the auscultatory waveforms; see Fig. 3. In addition, as BiLSTM layers provide the output layer with complete future and past context for every pulse in the feature vectors sequence, without displacing them from their relevant targets, the models including BiLSTM layers can more accurately identify the pulse associated with

This article has been accepted for publication in a future issue of this journal, but has not been fully edited. Content may change prior to final publication. Citation information: DOI 10.1109/JBHI.2020.3012567, IEEE Journal of Biomedical and Health Informatics

TABLE II
PERFORMANCE OF DIFFERENT MODELS IN DETERMINING SYSTOLIC AND DIASTOLIC BLOOD PRESSURE USING TIME-FREQUENCY FEATURES EXTRACTED FROM AUSCULTATORY WAVEFORM, ENERGY AND THE CORRESPONDING APPROXIMATE AND DETAIL DECOMPOSED PARTS ACHIEVED BY WAVELET PACKET DECOMPOSITION.

First Step Classification	Second Step Classification	Absolute Difference (%) ≤ 5	≤ 10	≤ 15	ME (mmHg)	MAE (mmHg)	SDE (mmHg)	BHS Grade	AAMI Standard
Systolic Blood Pressure									
Model 1	-	82.1	95.1	98.3	-0.5	2.0	4.3	A	Pass
Model 2	-	82.6	97.7	99.7	0.3	2.0	3.7	A	Pass
Model 3	-	83.4	97.4	99.4	0.0	1.9	3.9	A	Pass
Model 4	-	82.9	96.9	99.5	0.2	2.0	3.9	A	Pass
Model 5*	-	**86.3**	**97.4**	**99.1**	**0.2**	**1.7**	**3.7**	**A**	**Pass**
Model 5 with LOOCV	-	86.9	98.3	99.7	-0.4	1.5	3.5	A	Pass
Model 5 with LOSOCV	-	84.9	97.2	99.2	-0.2	1.8	4.1	A	Pass
Model 6	-	76.6	89.6	92.8	1.5	5.2	11.6	B	Fail
Model 7	-	80.3	91.3	95.4	0.7	3.2	8.8	A	Fail
DBN-DNN	-	79.5	87.0	91.3	3.1	4.5	12.2	B	Fail
DBN-DNN	DBN-DNN	85.0	94.8	96.8	0.5	2.3	6.9	A	Pass
FFNN	-	37.3	78.9	90.2	-7.6	7.6	5.4	D	Fail
FFNN	FFNN	76.0	93.6	97.4	-1.6	0.9	5.5	A	Pass
LSTM with features in [13]	-	79.7	92.3	96.0	-1.7	2.5	4.8	A	Pass
Diastolic Blood Pressure									
Model 1	-	71.0	91.3	97.7	0.8	3.8	5.6	A	Pass
Model 2	-	72.9	92.7	98.9	-0.7	3.7	5.1	A	Pass
Model 3	-	70.1	92.9	98.9	-0.1	3.6	5.2	A	Pass
Model 4	-	72.0	93.4	98.0	0.2	3.7	5.3	A	Pass
Model 5*	-	**74.0**	**93.4**	**99.2**	**-0.1**	**3.4**	**5.0**	**A**	**Pass**
Model 5 with LOOCV	-	76.6	93.4	98.3	0.7	3.4	5.3	A	Pass
Model 5 with LOSOCV	-	74.0	92.1	97.3	0.7	3.7	5.7	A	Pass
Model 6	-	65.2	87.9	93.5	-4.0	4.2	5.9	B	Pass
Model 7	-	70.0	89.6	97.4	0.2	4.1	5.7	A	Pass
DBN-DNN	-	67.9	85.8	92.2	-1.0	4.6	8.0	B	Fail
DBN-DNN	DBN-DNN	73.7	91.3	95.7	0.8	3.5	5.9	A	Pass
FFNN	-	33.2	74.0	89.6	6.9	8.1	6.9	D	Fail
FFNN	FFNN	67.3	90.7	98.0	-0.5	4.2	5.8	A	Pass
LSTM with features in [13]	-	63.7	84.7	95.9	1.6	3.9	6.6	A	Pass

* shows the best result, ME: Mean Error, MAE: Mean Absolute Error, SDE: Standard Deviation of Error, BHS: British Hypertension Society, AAMI: Association for the Advancement of Medical Instrumentation, LOOCV: Leave-One-Out Cross Validation, and LOSOCV: Leave-One-Subject-Out Cross Validation.

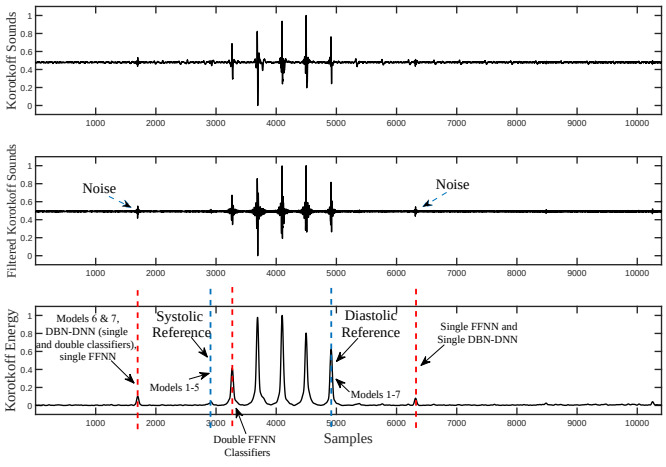

Fig. 3. An example of noise in an auscultatory waveform, which illustrates the reason for the better performance of the BiLSTM-RNN models and the two-step classification methods relative to the undirectional LSTM-RNNs or single step DBN-DNN and FFNN.

the SBP even in the presence of various noise in the Korotkoff sounds sequence. BiRNNs have previously been used and given improved results in domains such as sequence labeling in speech processing [39], translation [40], handwriting recognition [41], protein secondary structure prediction [42], and aligned with the literature, it was found that LSTM-RNNs including BiLSTM layers consistently outperform undirectional RNNs at sequence labeling in the specific application of SBP and DBP estimation from auscultatory waveforms.

On the other hand, while the best results were achieved by RNN models, the devised DBN-DNN classification model, which assumes the consecutive pulses (sounds) are independent, could not achieve acceptable results in terms of SDE (SDE = 12.2 and 8.0 mmHg for SBP and DBP, respectively) and could not pass the AAMI standard. The devised FFNN classifier was also unable to estimate NIBP accurately and poor results were obtained in terms of MAE (MAE = 7.6 and 8.1 mmHg for SBP and DBP, respectively). To increase the accuracy of the DBN-DNN and FFNN classification models in the presence of various noise, a second classification model was used to re-classify each AW beat. The inputs to the second classification model were formed from the output sequence of the first classifier. $\mathcal{N} = 3$ consecutive elements of the output sequence were concatenated to form a $2\mathcal{N} = 6$ input vector for the second classifier, as shown in Fig. 4. The second model works in a cascaded structure with the first model and was trained after completing the training of the first model using the inputs formed from the training output sequences of the

This article has been accepted for publication in a future issue of this journal, but has not been fully edited. Content may change prior to final publication. Citation information: DOI 10.1109/JBHI.2020.3012567, IEEE Journal of Biomedical and Health Informatics

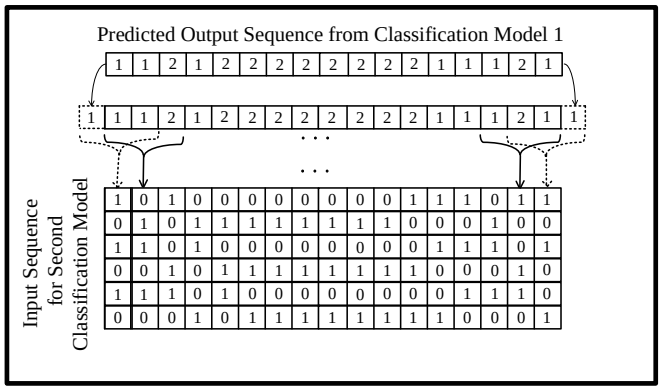

Fig. 4. An illustration of input and output sequence preparation for the second classification model, using $\mathscr{N} = 3$ consecutive elements of the output sequence from the first classification model. The input dimension is $2\mathscr{N} = 6$.

first classifier (explained above and shown in Fig. 4), and the training labels used to train the first classification model. As evident from Table II, the proposed second classification model had a remarkable positive impact in improving the BP estimation accuracy, as it is capable of coping with the beat misclassifications occurring due to motion artifact or sound noise in the measured Korotkoff sounds. However, none of the two-step classification models could outperform the devised BiLSTM-RNN models.

The existing AI-based approaches for NIBP estimation from AWs have two main problems. First, methods that assume Korotkoff sounds are temporally independent and thus classification models used are incapable of taking into account the temporal dependencies between consecutive Korotkoff sound sequences, cf. [24]. Second, whilst methods using undirectional LSTM-RNNs [13] or Gaussian mixture model-hidden Markov models (GMM-HMMs) [14] are able to capture the temporal information among segments of AWs, they can only make use of the previous context and not the future context. Hence, they are unable to deal with noise in AWs.

In the studies conducted in [27], [28], [43], it was shown that the manual auscultatory technique suffers from several possible inaccuracies, including the sensitivity of the stethoscope employed, the hearing acuity of the observer, the patient's anatomy, and the morphology and intensity of the Korotkoff sound. The inaccuracy of the manual auscultatory technique can also be caused by the unclear or indistinct Korotkoff sounds at SBP and DBP. The BiLSTM-RNN method developed in this study can however estimate BP more accurately, using the time-frequency features extracted from segments of AWs, as it can (1) recognize the difference between noise in a frame and a real Korotkoff sound, and further (2) detect indistinct Korotkoff sounds at SBP and DBP.

As shown in [44] the highest frequency component of Korotkoff sounds can be close to 400 Hz but with very low energy. Nevertheless, the sampling frequency of 500 Hz used in this study to digitize the Korotkoff sounds is not problematic, as phases I and IV (and V), that are related to systolic and diastolic beats, have frequencies less than 250 and 100 Hz, respectively. Furthermore, it is shown that a wide range of stethoscopes amplify sounds below 100 Hz and attenuate sounds above 200 Hz [45]. Also, as previously stated, the systolic and diastolic beats are related to the appearance and disappearance of the high frequency component, namely K_2 [29]. It should also be noted that the aim of this study was to develop an automated auscultatory BP estimation algorithm using deep learning, which in fact requires to detect systolic and diastolic beats and not the phase transitions, and hence the sampling frequency used is sufficient for this goal.

One limitation of this work is that, during the segmentation of AWs, it is assumed that a parallel OW is available and a frame of 1 s (500 samples) centered with each oscillometric peak was used to convert the AWs into the variable length sequences of segments. In future work, a more advanced segmentation technique needs to be developed which does not require OWs and a preprocessing step to detect oscillometric pulses and the corresponding peaks. In addition, convolutional layers which are able to optimally extract features can be used rather than the proposed manual feature extraction method to minimize the preprocessing required to prepare the data for the classification models.

VI. Conclusion

While a number of AI-based models have been proposed in the literature for automated BP estimation from AW, these methods either do not take into account the temporal dependencies between consecutive Korotkoff sound sequences or cannot use the future context and thereby deal with noise in AWs. In this study, the BP estimation problem from AWs was first converted to a sequence-to-sequence classification problem. To do this, a novel feature extraction technique was developed to extract time-frequency domain features from segments of Korotkoff sound sequences. A deep BiLSTM-RNN-based method was also developed that can label the features extracted from a sequence of segments formed from AWs. The SBP and DBP are then estimated by mapping the segments at which the sequence switches from one phase (between systolic and diastolic or otherwise) to another phase, to the deflation curve. To the best of our knowledge, this is the first study to develop an automated NIBP estimation method from Korotkoff sounds using BiLSTM-RNNs.

References

[1] B. V. Scheer, A. Perel, and U. J. Pfeiffer, "Clinical review: complications and risk factors of peripheral arterial catheters used for haemodynamic monitoring in anaesthesia and intensive care medicine," *Critical Care*, vol. 6, no. 3, p. 199, 2002.

[2] M. Semret, M. Zidehsarai, and R. Agarwal, "Accuracy of oscillometric blood pressure monitoring with concurrent auscultatory blood pressure in hemodialysis patients," *Blood Pressure Monitoring*, vol. 10, no. 5, pp. 249–255, 2005.

[3] J. Landgraf, S. H. Wishner, and R. A. Kloner, "Comparison of automated oscillometric versus auscultatory blood pressure measurement," *The American Journal of Cardiology*, vol. 106, no. 3, pp. 386–388, 2010.

[4] E. O'Brien, J. Petrie, W. A. Littler, M. de Swiet, P. L. Padfield, K. O'malley, M. Jamieson, D. Altman, M. Bland, and N. Atkins, "The British Hypertension Society protocol for the evaluation of automated and semi-automated blood pressure measuring devices with special reference to ambulatory systems," *Journal of Hypertension*, vol. 8, no. 7, pp. 607–619, 1990.

[5] J. Moraes, M. Cerulli, and P. Ng, "A strategy for determination of systolic, mean and diastolic blood pressures from oscillometric pulse profiles," in *Computers in Cardiology 2000*. IEEE, 2000, pp. 211–214.

[6] B. G. Celler, A. Argha, P. N. Le, and E. Ambikairajah, "Novel methods of testing and calibration of oscillometric blood pressure monitors," *PloS One*, vol. 13, no. 8, p. e0201123, 2018.

[7] B. G. Celler, P. N. Le, A. Argha, and E. Ambikairajah, "GMM-HMM based blood pressure estimation using time domain features," *IEEE Transactions on Instrumentation and Measurement*, 2019.

[8] A. Argha and B. G. Celler, "Blood pressure estimation from time domain features of oscillometric waveforms using long-short-term-memory recurrent neural networks," *IEEE Transactions on Instrumentation and Measurement*, 2019.

[9] H. Skirton, W. Chamberlain, C. Lawson, H. Ryan, and E. Young, "A systematic review of variability and reliability of manual and automated blood pressure readings," *Journal of Clinical Nursing*, vol. 20, no. 5-6, pp. 602–614, 2011.

[10] K.-G. Ng and C. F. Small, "Survey of automated noninvasive blood pressure monitors." *Journal of Clinical Engineering*, vol. 19, no. 6, pp. 452–475, 1994.

[11] A. K. Gupta, A. Maheshwari, D. D. Tresch, and R. K. Thakur, "Cardiac arrhythmias in the elderly," *Cardiac Electrophysiology Review*, vol. 6, no. 1-2, pp. 120–128, 2002.

[12] M. J. Cleland, B. Pham, and D. R. Miller, "Influence of arrhythmias on accuracy of non-invasive blood pressure monitors," *Canadian Journal of Anaesthesia*, vol. 45, no. 7, pp. 699–705, 1998.

[13] A. Argha and B. G. Celler, "Blood pressure estimation using time domain features of auscultatory waveforms and deep learning," in *2019 41st Annual International Conference of the IEEE Engineering in Medicine and Biology Society (EMBC)*. IEEE, 2019, pp. 1821–1824.

[14] B. G. Celler, P. N. Le, A. Argha, and E. Ambikairajah, "Blood pressure estimation using time domain features of auscultatory waveforms and gmm-hmm classification approach," in *2019 41st Annual International Conference of the IEEE Engineering in Medicine and Biology Society (EMBC)*. IEEE, 2019, pp. 208–211.

[15] S. Lee, J.-H. Chang, S. W. Nam, C. Lim, S. Rajan, H. R. Dajani, and V. Z. Groza, "Oscillometric blood pressure estimation based on maximum amplitude algorithm employing Gaussian mixture regression," *IEEE Transactions on Instrumentation and Measurement*, vol. 62, no. 12, pp. 3387–3389, 2013.

[16] P. K. Lim, S.-C. Ng, W. A. Jassim, S. J. Redmond, M. Zilany, A. Avolio, E. Lim, M. P. Tan, and N. H. Lovell, "Improved measurement of blood pressure by extraction of characteristic features from the cuff oscillometric waveform," *Sensors*, vol. 15, no. 6, pp. 14 142–14 161, 2015.

[17] M. Forouzanfar, H. Dajani, V. Groza, M. Bolic, and S. Rajan, "Comparison of feed-forward neural network training algorithms for oscillometric blood pressure estimation," in *4th International Workshop on Soft Computing Applications*. IEEE, 2010, pp. 119–123.

[18] S. Lee and J.-H. Chang, "Oscillometric blood pressure estimation based on deep learning," *IEEE Transactions on Industrial Informatics*, vol. 13, no. 2, pp. 461–472, 2017.

[19] A. Argha, J. Wu, S. W. Su, and B. G. Celler, "Blood pressure estimation from beat-by-beat time-domain features of oscillometric waveforms using deep-neural-network classification models," *IEEE Access*, vol. 7, pp. 113 427–113 439, 2019.

[20] G. Chu, Z. Zhang, M. Xu, D. Huang, and Q. Dai, "Validation of a smartphone auscultatory blood pressure kit Accutension XYZ-110 in adults according to the ANSI/AAMI/ISO 81060-2: 2013 standard," *Blood Pressure Monitoring*, vol. 22, no. 5, pp. 290–294, 2017.

[21] B. S. Alpert, "The accutension stetho, an automated auscultatory device to validate automated sphygmomanometer readings in individual patients," *Journal of Human Hypertension*, vol. 32, no. 6, pp. 455–459, 2018.

[22] H. Wu, B. Wang, X. Zhu, G. Chu, and Z. Zhang, "A new automatic blood pressure kit auscultates for accurate reading with a smartphone: a diagnostic accuracy study," *Medicine*, vol. 95, no. 32, 2016.

[23] Z. Zhang, W. Xi, B. Wang, G. Chu, and F. Wang, "A convenient method to verify the accuracy of oscillometric blood pressure monitors by the auscultatory method: A smartphone-based app," *The Journal of Clinical Hypertension*, vol. 21, no. 2, pp. 173–180, 2019.

[24] F. Pan, P. He, C. Liu, T. Li, A. Murray, and D. Zheng, "Variation of the korotkoff stethoscope sounds during blood pressure measurement: Analysis using a convolutional neural network," *IEEE Journal of Biomedical and Health Informatics*, vol. 21, no. 6, pp. 1593–1598, 2017.

[25] S. G. Rabinovich, *Measurement errors and uncertainties: theory and practice*. Springer Science & Business Media, 2006.

[26] E. O'Brien, J. Petrie, W. Littler, M. de Swiet, P. L. Padfield, D. Altman, M. Bland, A. Coats, N. Atkins *et al.*, "The British Hypertension Society protocol for the evaluation of blood pressure measuring devices," *Journal of Hypertension*, vol. 11, no. Suppl 2, pp. S43–S62, 1993.

[27] B. G. Celler, P. Le, J. Basilakis, and E. Ambikairajah, "Improving the quality and accuracy of non-invasive blood pressure measurement by visual inspection and automated signal processing of the korotkoff sounds," *Physiological Measurement*, vol. 38, no. 6, p. 1006, 2017.

[28] B. G. Celler, J. Basilakis, K. Goozee, and E. Ambikairajah, "Non-invasive measurement of blood pressure-why we should look at BP traces rather than listen to korotkoff sounds," in *Engineering in Medicine and Biology Society (EMBC), 2015 37th Annual International Conference of the IEEE*. IEEE, 2015, pp. 5964–5967.

[29] S. G. Blank, J. E. West, F. Müller, R. J. Cody, G. A. Harshfield, M. S. Pecker, J. Laragh, and T. G. Pickering, "Wideband external pulse recording during cuff deflation: a new technique for evaluation of the arterial pressure pulse and measurement of blood pressure," *Circulation*, vol. 77, no. 6, pp. 1297–1305, 1988.

[30] R. H. Bailey and J. H. Bauer, "A review of common errors in the indirect measurement of blood pressure: sphygmomanometry," *Archives of internal medicine*, vol. 153, no. 24, pp. 2741–2748, 1993.

[31] A. Burton, "The criterion for diastolic pressure-revolution and counter-revolution," *Circulation*, vol. 36, no. 6, pp. 805–809, 1967.

[32] D. E. Rumelhart, G. E. Hinton, and R. J. Williams, "Learning internal representations by error propagation," California Univ San Diego La Jolla Inst for Cognitive Science, Tech. Rep., 1985.

[33] S. Hochreiter and J. Schmidhuber, "Using recurrent neural network models for early detection of heart failure onset," *Journal of the American Medical Informatics Association*, vol. 9, no. 8, pp. 1735–1780, 1997.

[34] M. Schuster and K. K. Paliwal, "Bidirectional recurrent neural networks," *IEEE Transactions on Signal Processing*, vol. 45, no. 11, pp. 2673–2681, 1997.

[35] A. Graves, A.-r. Mohamed, and G. Hinton, "Speech recognition with deep recurrent neural networks," in *2013 IEEE international conference on acoustics, speech and signal processing*. IEEE, 2013, pp. 6645–6649.

[36] G. E. Hinton, S. Osindero, and Y.-W. Teh, "A fast learning algorithm for deep belief nets," *Neural Computation*, vol. 18, no. 7, pp. 1527–1554, 2006.

[37] M. Forouzanfar, H. R. Dajani, V. Z. Groza, M. Bolic, and S. Rajan, "Feature-based neural network approach for oscillometric blood pressure estimation," *IEEE Transactions on Instrumentation and Measurement*, vol. 60, no. 8, pp. 2786–2796, 2011.

[38] Y. Wu, M. Schuster, Z. Chen, Q. V. Le, M. Norouzi, W. Macherey, M. Krikun, Y. Cao, Q. Gao, K. Macherey *et al.*, "Google's neural machine translation system: Bridging the gap between human and machine translation," *arXiv preprint arXiv:1609.08144*, 2016.

[39] M. Schuster, "On supervised learning from sequential data with applications for speech recognition," *Daktaro disertacija, Nara Institute of Science and Technology*, 1999.

[40] M. Sundermeyer, T. Alkhouli, J. Wuebker, and H. Ney, "Translation modeling with bidirectional recurrent neural networks," in *Proceedings of the 2014 Conference on Empirical Methods in Natural Language Processing (EMNLP)*, 2014, pp. 14–25.

[41] M. Liwicki, A. Graves, S. Fernàndez, H. Bunke, and J. Schmidhuber, "A novel approach to on-line handwriting recognition based on bidirectional long short-term memory networks," in *Proceedings of the 9th International Conference on Document Analysis and Recognition, ICDAR 2007*, 2007.

[42] G. Pollastri and A. Mclysaght, "Porter: a new, accurate server for protein secondary structure prediction," *Bioinformatics*, vol. 21, no. 8, pp. 1719–1720, 2005.

[43] D. Zheng, R. Giovannini, and A. Murray, "Effect of respiration, talking and small body movements on blood pressure measurement," *Journal of Human Hypertension*, vol. 26, no. 7, p. 458, 2012.

[44] J. Allen, T. Gehrke, J. J. O'Sullivan, S. T. King, and A. Murray, "Characterization of the korotkoff sounds using joint time–frequency analysis," *Physiological measurement*, vol. 25, no. 1, p. 107, 2003.

[45] "Non-invasive sphygmomanometers – part 2: Clinical validation of automated measurement type," *ANSI/AAMI/ISO 81060-2 Standard*, 2009.

Ahmadreza Argha received the B.S. and M.S. degrees in Electrical Engineering from Shiraz University, and the PhD from UTS, Australia. He is currently a Postdoctoral Research Fellow in the Graduate School of Biomedical Engineering, UNSW, Sydney, Australia. His current research interests include robust control, fault tolerant control, network systems, human-in-the-loop control systems, biomedical signal processing and machine learning applications in biomedical engineering.

Branko G. Celler (M'80-SM'02-F'04) received his BSc in Physics and Computer Science in 1969, his BEE (Major in Control) in 1971 and his PhD in Biomedical Engineering in 1978. He subsequently completed a Postdoctoral Fellowship at the Johns Hopkins School of Medicine (1978-1980) before returning to Australia to take up an academic position at the UNSW. He established and led the Biomedical Systems Laboratory within the School of Electrical Engineering and Telecommunications from 1981-2006, was appointed full professor in 1997 and was Head of School from 1998-2006. He has published over 300 refereed Journal Papers and Conference Proceedings as well as 14 Book Chapters and has received more than $15m in competitive national research funding. His research interests include biomedical instrumentation and signal processing, bioinformatics and decision support systems as applied to telehealth systems for the management of chronic disease in the home and the community. He is internationally recognised for his work on the development of telehealth technologies and services for the management of chronic conditions in the community. Prof. Celler is a Fellow of the IEEE, a Fellow of the Australian Academy of Technological Science and Engineering, a Fellow of the Australian Institute of Engineers and a Foundation Fellow of the Australian College of Health Informatics. He is an Emeritus Professor at the UNSW.

Nigel H. Lovell is currently at the Graduate School of Biomedical Engineering UNSW Sydney where he holds a position of Scientia Professor and Head of School. His research work has covered areas of expertise ranging from cardiac and retinal modeling, medical informatics and data analytics especially related to telehealth technologies, biological signal processing, and visual prosthesis design. Much of his work has been in the design of appropriate technologies to restore sensory loss and to manage chronic disease and frailty. He has commercialised a range of telehealth technologies for managing chronic disease and falls in the older population. Prof Lovell has been awarded over $84 million in R&D funding. Over his career he has mentored 70 PhD students and delivered more than a hundred keynote presentations. He is a Fellow of seven learned academies and has been ranked as one of the top ten most published biomedical engineers in the world. For 2017 and 2018 he was the President of the world's largest biomedical engineering society - the IEEE Engineering in Medicine and Biology Society.